Optimized placement of parasitic vibration energy harvesters for autonomous structural health monitoring

Pearson MR, Featherston CA, Pullin R and Holford KM

School of Engineering, Cardiff University, Queens Buildings, The Parade, Cardiff, CF24 3AA, UK

Abstract

Energy harvesting, based on sources including vibration and thermal gradients has been exploited in recent years to power telemetry, small devices or to charge batteries or capacitors. Generating the higher levels of power which have thus far been required to run sensor systems such as those needed for structural health monitoring (SHM) has been more challenging. In addition, harvesters such as those required to capture vibration, often require additional elements (e.g. cantilevers) to be added to the structure, and harvest over a relatively narrow band of frequencies. In aerospace applications, where weight is at a premium and vibrations occur over a broader range of frequencies this is non-ideal. With the advent of new, lower power monitoring systems the potential for energy harvesting to be utilized is significantly increased. This paper optimizes the placement of a set of parasitic piezoelectric patches to harvest over the broad band of frequencies found in an aircraft wing and validates the results experimentally. Results are compared with the requirements of a low power SHM system, with a closing of the gap between the energy generated and that required being demonstrated.

Keywords:

Energy harvesting, piezoelectric, vibration, structural health monitoring, optimization, genetic algorithm (GA).

Introduction

Autonomous SHM systems are becoming a real possibility for monitoring aircraft structures, providing early detection of the deterioration of a structure and potentially an assessment of damage severity and remaining life. However to avoid the weight and complexity burden of additional wiring these systems would require an architecture of wireless sensor nodes (WSNs). These nodes would require processing, data storage and wireless communication capabilities to become truly autonomous. Depending on the operational strategy of these nodes (sampling rate, processing capabilities) power requirements will vary. Various nodes have been developed in the literature differing in complexity from simple temperature monitoring to full SHM monitoring.

Many examples of WSNs are based on a modular approach. Wu et al. 2007 used a transducer input unit, a data processing core and wireless communications to monitor output from piezoelectric transducers or strain gauges. Estimated power was 30mW however in sleep this was reduced to just over 1mW. A wireless impedance based SHM node was developed by Mascarenas et al (2007) with a micro controller and an Xbee radio for wireless communications. In sleep mode the power requirement was 51μW however the maximum power consumption could be as large as 212.85mW. Zhou et al (2009) were able to reduce the power consumption of a wireless transducer node by removing the need for digital/analogue converters (DACs/ADCs). The node consumed 0.15mW in sleep mode, increasing to 18mW in active mode with the radio off, but 70mW when transmitting. Wireless transducer nodes have also been developed that can detect the deterioration of a structure using impedance and Lamb wave approaches (Kim et al. 2009) however the increased complexity of the node raises the power requirements due to the additional circuitry.

For these transducer nodes to be truly autonomous they would require a power source. Batteries have a finite lifetime and even though this can be several years they require replacing, incurring a large amount of maintenance and hence cost. They may also be inaccessible. An alternative is to apply energy harvesting techniques, such as the use of vibration and thermal gradients which can be harvested using piezoelectric and thermoelectric generators. This paper focuses on the viability of using vibration due to its availability throughout the flight cycle.

Piezoelectric harvesters generally take the form of cantilever beams with or without tip masses (which are used to tune the harvesters to particular frequencies in a unimorph (one piezoelectric layer) or bi-morph (two layers either side of the substrate) configuration. Zhu and Edkins (2011) developed a simple model for the evaluation of piezoelectric energy harvesting devices incorporating backwards coupling which has a large effect on the power output, generated voltage and tip displacement. Ng and Liao (2005) developed three types of cantilever, two bi-morph configurations with the piezoelectric layers connected in parallel and then in series and a unimorph cantilever. Constitutive piezoelectric equations used to predict their performance found the series cantilever generated the greatest power for higher frequencies/loads and therefore had the largest operating bandwidth. Ly et al (2011) developed a model for piezoelectric cantilevers based on Euler-Bernoulli beam theory. The model could be used for multiple

resonant frequencies, broadening the beam's response and was validated with experimental investigations with good agreement observed between the two. Microelectromechanical systems (MEMS) have also been developed which include piezoelectric energy harvesting devices on a miniature scale. Fang et al (2006) developed a MEMS cantilever device with a peak power of 2.16μW. Liu et al (2011) fabricated a MEMS based piezoelectric cantilever energy harvester with a low resonant frequency consisting of 10 piezoelectric rectangular films on a supporting beam with a silicon proof mass giving a power output of 11.6nW for a matched load of 333kΩ.

For vibrations which are more broadband in nature Ferrari et al (2010) showed numerical and experimental investigations of a non-linear piezoelectric cantilever. A PZT substrate was applied to steel cantilevers using a screen printing technique. A permanent magnet was placed at the tip of the beam with an opposing polarity magnet located at various different distances from the tip of the beam to achieve a bi-stable state and a marked improvement in open circuit voltage over a much wider bandwidth. Karami et al (2013) developed a small scale nonlinear wind turbine using bi-morph piezoelectric cantilevers again using magnets to achieve a bi-stability and increase the power output over a wider bandwidth.

Research has also looked at the use of commercially available piezoelectric elements. Sodano et al (2005) assessed three types of piezoelectric cantilevers for charging nickel metal hydride batteries using a monolithic PZT patch on an aluminium substrate cantilever, a MFC also on an aluminium substrate cantilever and a Quickpack bimorph cantilever made up of four piezoelectric rectangular monolithic sheets demonstrating the power generated was greatest with the PZT cantilever. He also examined interdigitated electrodes (IDE) and piezo-composite designs (Sodano et al (2006)) demonstrating that the performance of an IDE is more dependent on its structure than the piezoeceramic fibers used and that although the power generated was less for an IDE device, it was able to generate higher voltages with the compressive stresses induced and was likely to result in devices with longer lives than those in which tensile stresses are prevalent (Chidambaram et al. 2012).

There are many practical applications or scenarios where piezoelectric materials could be used to provide a power source for wireless transducer nodes. Pasquale et al (2011) developed a piezoceramic cantilever consisting of a 200μm piezoceramic layers on a PVC substrate for harvesting vibration energy for railway vehicles. Testing on a scale model of a carriage at resonance generated a peak power of 4mW which was stored in a battery and used to power two axis accelerometers and an RF transmitter. Zhu et al (2011) developed a credit card sized wireless transducer node that incorporated a T-shaped piezoelectric bimorph cantilever with temperature and pressure transducers, a 3-axis accelerometer, a micro-controller and an RF transmitter with energy storage within a single unit, generating 240μW of power at a resonant frequency of 66Hz for a 0.4g vibration. Ertuk et al (2009) developed an electromechanical model for a load bearing multifunctional wing spar for unmanned aerial vehicles. Results showed that 4.1mW/g^2 could be generated for a match load of 32kΩ. However a theoretical structural analysis found the multifunctional wing spar had much lower strength than the original wing spar with the same dimensions. Further development incorporated solid state batteries and a

transducer node (Anton et al. 2012). Regulated power during testing was 1.5mW. A mathematical model was produced to determine the effects of adding solar and piezoelectric energy harvesting to a UAV's flight endurance (i.e. the length of time the UAV could fly for) (Anton and Inman 2011). The model was coupled with experimental results for power harvested during typical UAV manoeuvres conducted on a sunny day. Results showed that a flexible solar panel increased the flight endurance by 0.7% if the weight of the additional solar panels was removed from the structural weight. Adding the weight of the piezoelectric panels only decreased flight endurance no matter how much structural mass was removed. This shows the necessity of considering the possible adverse effects of adding energy harvester devices to certain structures.

An alternative to the use of cantilevers is to place piezoelectric energy harvesters directly onto the structure. In this case determination of the optimal placement is essential to achieving maximum power generation. Bachmann et al (2012) focused on the placement of piezoelectric patches in complex real world structures for maximizing the harvested strain energy, using a finite element model to predict the strain in complex composite materials followed by an exhaustive placement search, assuming that the introduction of the patch does not alter the modal behavior and the planar piezoelectric coupling coefficient. Liao and Sodano (2012) developed an electromechanical model and loss analysis to determine optimum placement of piezoelectric patches on cantilever beams demonstrating a maximum patch size beyond which increases in size do not result in improved performance.

In this work we determine the output derived from the optimal placement of a set of four commercially available piezoelectric elements (with the possibility to optimize the number of harvesters at a later date) mounted on a specimen representative of an aircraft wing panel subject to the level of vibration typically generated during flight using a Genetic Algorithm based optimization process which aims to maximize strain across the broad band of frequencies experienced, to determine the feasibility of using this to power a SHM node.

Optimized harvesting using directly mounted piezoelectric elements

The potential power which can be generated using a piezoelectric harvester is directly proportional to the strain generated within the harvester, a function of the vibration characteristics (curvature, amplitude, frequency etc.) of the panel to which it is bonded and the orientation of the transducer with respect to the direction of strain in the panel. The maximum power output will be achieved by a harvester placed at the position on the panel that experiences the greatest strain during vibration which therefore needs to be identified. However, the vibration of such a system is a complex function of the forces acting upon it, its geometry and its boundary conditions. Additional complexity is added in the case of an aircraft wing panel for example due to the continually changing conditions it experiences where the vibration characteristics are inhomogeneous throughout all stages of flight and along the length of the wing. As a result of these continuously changing conditions a range of frequencies and amplitudes must be

considered and the point that experiences the greatest strain across all the vibration frequencies should be identified for energy harvesting. In this work an objective function, based on maximizing strain across the range of frequencies and acceleration levels experienced by a simplified aircraft wing panel is used in combination with a Genetic Algorithm to optimize the location and orientation of a set of harvesters. The problem is solved for the particular case of a metallic rectangular panel, built in along all four edges, however the methodology applied could be adapted for different materials, geometries and boundary conditions.

Strain in a vibrating built-in plate

Deflection profile

For a plate with built-in edges, the deflection profile must satisfy two conditions; the deflection along the edge must be zero and the tangential plane to the deflected middle surface along the edge must coincide with the initial position of the middle plane. Therefore $w = \frac{\partial w}{\partial x} = 0$ at $x = 0, a$ and $w = \frac{\partial w}{\partial y} = 0$ at $y = 0, b$ (Timoshenko et al (1959). Consequently for a plate with all four edges built-in under a vibrational load, the deflection of the plate is described by

$$w = \frac{w_0}{4}\left(1 - \cos\frac{2m\pi x}{a}\right)\left(1 - \cos\frac{2n\pi y}{b}\right) \qquad (1)$$

where w_o is the maximum amplitude, a and b are the dimensional length and width of the plate respectively, and m and n are the number of half wave lengths in the x (length) and y (width) directions.

Strain in a plate under small deflections

Since the power output of a piezoelectric energy harvester is related to the level of strain, the first stage in the optimization process is to determine the strain at the different locations and orientations within the plate at which the harvester could be mounted. Two types of strain are generated in a plate when it is deformed; bending strain which assumes the neutral axis (mid-plane of the plate) remains unstrained throughout the deformation and the maximum strain occurs at the surface, and membrane strain which considers only strain in the mid-plane. Both will be considered here, although for small deflections the bending strain will be significantly larger.

Bending strain

Assuming small deflections, with the plate material not exceeding its elastic limit, the bending strain, experienced throughout the thickness of the plate based on simplifying the deflection profile of the plate to:

.

$$w = w_0\left(\sin^2\frac{m\pi x}{a}\right)\left(\sin^2\frac{n\pi y}{b}\right) \qquad (2)$$

is given by (Timoshenko et al (1959)) :

$$\varepsilon_{Bx} = \frac{t}{2}\left[w_0\left(\frac{2m\pi}{a}\right)^2 \cos\left(\frac{2m\pi x}{a}\right)\sin^2\frac{n\pi y}{b}\right]$$

$$\varepsilon_{By} = \frac{t}{2}\left[w_0\left(\frac{2n\pi}{b}\right)^2 \cos\left(\frac{2n\pi y}{b}\right)\sin^2\frac{m\pi x}{a}\right] \quad (3)$$

Membrane strain

The membrane strain (ε_{Mi}), again based on the simplified expression for deformation can be described by:

$$\varepsilon_{Mx} = \frac{1}{2}\left[w_0\left(\frac{2m\pi}{a}\right)^2 \cos\left(\frac{2m\pi x}{a}\right)\sin^2\frac{n\pi y}{b}\right]^2$$

$$\varepsilon_{My} = \frac{1}{2}\left[w_0\left(\frac{2n\pi}{b}\right)^2 \cos\left(\frac{2n\pi y}{b}\right)\sin^2\frac{m\pi x}{a}\right]^2 \quad (4)$$

Optimal position for harvester over a range of frequencies

The optimal position for a piezoelectric energy harvester on a deflecting plate is the area that experiences the maximum bending plus membrane strain, where for a rectangular plate with built-in edges this can be determined for a specific frequency by equations (3) and (4). However, in terms of an aircraft wing panel, considering the maximum strain for just one frequency is unrealistic as the vibration frequency and hence mode shapes are variable throughout flight and therefore the optimal position at one vibration frequency may not be favorable at another. With this in mind, the optimal positioning for a piezoelectric transducer(s) on an aircraft wing panel must take into consideration its vibration characteristics over a range of frequencies. The point of the panel that experiences the greatest strain over the entire frequency range during flight will therefore be the optimal position and hence should be established. This can be determined by finding the strain generated over the frequency range from zero to the maximum frequency (ω_{max}). This is shown in equations (5) and (6) for membrane and bending strain respectively where *w*' and *w*'' are the first and second derivatives of the deflection equation with respect to either the *x* or the *y* direction

$$F(x,y) = \iint_0^{\omega_{max}} \frac{1}{2}[w']^2 f \quad (5)$$

$$F(x,y) = \iint_0^{\omega_{max}} \frac{t}{2} w'' \omega \qquad (6)$$

In order to solve for the optimal position over a frequency range, the extent of this range and the resulting mode shapes experienced by the panel must first be determined.

Problem definition

Specimen design

The panel chosen for this study was based on that used by Jegley (1998) in a study of the loading of impact damaged wing box panels. Jegley‘s panel was cut from a wing box, representative of a section of a commercial transport aircraft wing, designed and manufactured by the McDonnell Douglas Aerospace Company for the purposes of loading to failure. The panel was made from Hercules, Inc. AS4/3501-6 carbon epoxy in 9 ply stacks. The dimensions and relevant properties of the panel are given in Table 1. An equivalent aluminium panel was designed for this study based on the dimensions of the Jegley panel. This was manufactured from 0.6mm aluminium alloy grade BS1470 6082-T6. In order to simplify the design of the specimen the stiffeners were not incorporated but their effect approximated by providing built in boundary conditions along all four edges of the panel.

Table 1. Characteristics of the replica wing panel

Notation	Property	SI Units	Value for Plate
a	Length of plate	mm	387
b	Width of plate	mm	254
t	Thickness of plate	mm	0.6
E	Modulus of elasticity	GPa	70
ν	Poisson Ratio	-	0.35

Deflection profile

To define the deflection profile and hence strain in the panel based on the equations outlined in the previous section, an indication of the amplitude and frequency of the vibrations typically found in an aerospace panel was then required.

Amplitude

The Engineering Sciences Data Unit (ESDU) aerodynamics document on structural design against fatigue ESDU (1996) states 'The primary sources of structural excitation are due to acoustic and aerodynamic generation although structurally transmitted vibration may have an additional influence.' Further to this, the same document identifies boundary layer turbulence as the primary source of vibration during flight for a typical aircraft wing panel. However, during take-off it is likely that jet noise will also contribute significantly to wing panel vibrations, and buffet may also contribute during flight.

It is possible to calculate the pressure fluctuations a wing panel will be subjected to due to boundary layer turbulence. Such pressure fluctuations calculated at a given position on a structure are dependent on altitude, Mach number (or velocity) and the distance behind the leading edge of the structure. To give a realistic range of pressure fluctuations for different types of aircraft, two examples were considered, a large passenger craft and a small unmanned aerial vehicle (UAV), taking a point at the rear edge of the wing (i.e. the furthest point from the leading edge). For the large passenger jet, a Boeing 777 was used, and for the UAV, an RQ-7 Shadow 200 was chosen. The relevant characteristics of both aircraft are given in Table 2.

Table 2. Characteristics of a large and a small aircraft for pressure fluctuation calculation

Aircraft	Cruise altitude (m)	Average cruise speed (km/h)	Mach number, M	Wing width (m)
Boeing 777 [14]	10670	900	0.84	7.96
Shadow 200 [15]	2400	110	0.1	0.3

These were used to determine suitable test parameters in conjunction with flight profiles. Pressure fluctuations at the rear edge of the wing up to a frequency of 350Hz (corresponding to the expected frequency range to which it was anticipated the panel would be subject discussed in the following section) were calculated for a series of values of altitude, Mach number, and distance behind the leading edge within the range set by the Boeing 777 and the Shadow 200. The calculations were made using the method from the ESDU (1968). The maximum pressure fluctuation within the range of values was found to be 22Pa. This was then used to calculate the deflection of the panel due to the fluctuating pressure, using calculations from the ESDU (1995). The results of these calculations suggest that amplitudes of up to ±0.1mm would be appropriate for a wing panel subject to boundary layer turbulence. To ensure that all possible vibration amplitudes were tested, including allowing for the effect of other vibration sources such as jet noise, a maximum amplitude of ±0.2mm was used.

Frequency range and mode shapes of an aircraft wing panel

The frequency range experienced by a typical wing panel was taken from data provided by an aircraft manufacturer. This data showed that although frequencies of up to 400 Hz were recorded, the magnitudes of vibrations above 350 Hz in comparison to those of the

lower frequencies are negligible and thus the energy harvesting potential above 350 Hz would be minimal. Therefore, only vibration frequencies of between 0 and 350 Hz will be considered.

The natural frequencies and corresponding mode shapes which occur in this frequency range for a plate with the properties presented in Table 1 have been determined using Finite Element Analysis (FEA) and are shown in Figure 1.

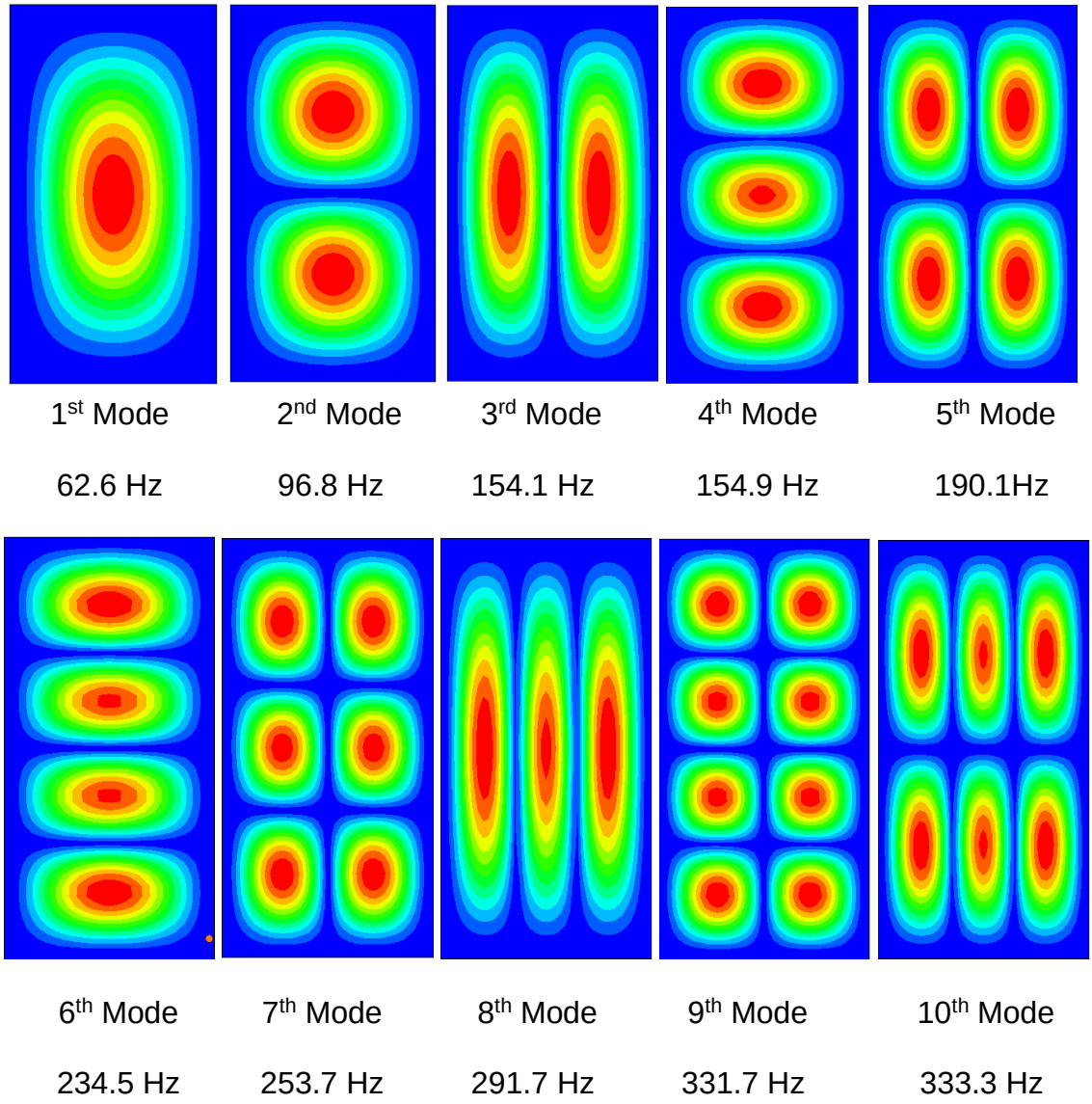

Figure 1. FEA simulations of the natural frequency mode shapes generated between 0-350Hz for a vibrating plate with the properties described in Table 1

Wireless SHM System

Indicative power requirements for the harvester were based on a system (developed by the authors (Grigg (2018)) based on Acoustic Emission (AE) and the use of nodes consisting of three piezoelectric sensors in a small array (75mm apart) (Figure 2). AE was selected as a passive monitoring technique with minimal power requirements which is able to detect, locate and characterize damage in both metallic and composite structures. The close spacing of the sensors removes the need for power intensive time synchronization between nodes, reduces excessive cabling and has been shown to perform well for artificial sources on a range of structures from simple plates to an A350 aircraft wing, with a high level of accuracy and repeatability shown. The sensor node has an operating power of around 16 mW and a sleep mode of 0.12mW.Whilst generation of the 16mW power level would allow the system to 'listen' for damage uninterruptedly, damage such as fatigue cracks will generate signals continuously which can be detected when the system is woken up having harvested sufficient energy. A power storage and management system also developed by the authors (Thangaraj (2017)) combines supercapacitor and solid state battery storage to provide low leakage storage combined with the quick response needed on wakeup to deliver the power to the system as needed.

Figure 2. Low power structural health monitoring system

Optimization

Objective function

From vibration theory it is known that as a panel is vibrated at each natural frequency, a distinctive mode shape will be generated. However, as the frequency deviates from that natural frequency, the mode shape will alter to a state between that of the initial natural frequency mode shape and that of the next natural frequency mode shape. Furthermore, this will also be affected by the profile of the driving displacement-which in this case will be an actuator attached to the center of the panel. This gives rise to a large variation and level of complexity in the vibrational mode shapes possible over the frequency range and therefore several approximations must be made in formulating the optimization problem.

Firstly, due to a lack of detailed information on the duration of different frequencies of vibration throughout a flight, it will be assumed that each frequency will operate for an equal length of time throughout the frequency range (e.g. 0 Hz = 1 sec, 0.1 Hz = 1 sec, 0.2 Hz = 1 sec, ... , 350 Hz = 1 sec). Given more detailed data the weighting factors could be easily modified to optimize for a particular set of conditions. Secondly, it will be assumed that the mode shapes generated at the natural frequencies will remain the same over a portion of the frequency range (α_{mn}), which will be assumed to extend between the mid-points between each pair of natural frequencies. For example, if the first three natural frequencies occur at 20, 50 and 60 Hz, the mode shape generated at 20 Hz would be assumed to occur between 0 and 35 Hz. Similarly, the mode shape generated at 50Hz would be assumed to occur between 35 and 55 Hz. This is illustrated in Figure 3.

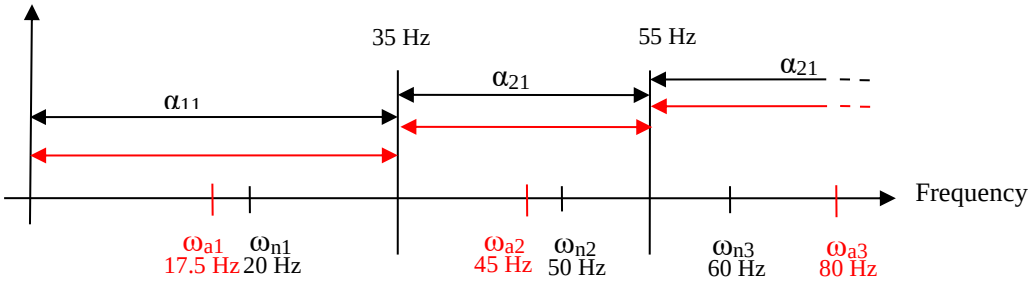

Figure 3. Weighting of mode shapes through the frequency range

The panel will be considered to take on each mode shape in turn, generating the associated amount of energy a number of times per second according to the frequency of the vibration. At the beginning of the frequency range this will be ω_{start} and by the end this will be ω_{finish}. In between these the number of times the plate deforms will vary linearly. Since the plate is assumed to exist at each frequency over the total test range i.e. 0 to 350Hz for an equal amount of time, the average number of times the plate will deform will be $(\omega_{start} + \omega_{finish})/2$. The total energy generated over this frequency range will therefore be $(\omega_{start} + \omega_{finish})/2$ multiplied by the energy generated in one cycle i.e. flat plate to mode shape positive to flat plate to mode shape negative to flat plate.

Following these assumptions the bending and membrane strain equations over the entire frequency range (equations (5) and (6)) can be rewritten as

$$F(x,y) = \sum_m \sum_n \alpha_{mn} \frac{t}{2} w'' \omega_a \tag{7}$$

$$F(x,y) = \sum_m \sum_n \alpha_{mn} \frac{1}{2} [w']^2 \omega_a \tag{8}$$

where the vibration variables α_{mn} and ω_a can be determined from Figure 3, and hence equations (7) and (8) can be solved. The vibration variables for the plate are shown in Table 3.

Table 3. Assumed frequency weightings used for plate optimisation.

Mode Shape	Natural Frequency (Hz)	Mode		Frequency Range (Hz)		Frequency Weighting	
	ω_n	m	n	Minimum	Maximum	α_{mn}	ω_m
1st	62.6	1	1	0	79.7	79.7	39.85
2nd	96.8	2	1	79.71	125.5	45.79	102.605
3rd	154.1	1	2	125.51	154.5	28.99	140.005
4th	154.9	3	1	154.51	172.5	17.99	163.505
5th	190.1	2	2	172.51	212.3	39.79	192.405
6th	234.5	4	1	212.31	244.1	31.79	228.205
7th	253.7	3	2	244.11	272.7	28.59	258.405
8th	291.7	1	3	272.71	300	27.29	286.355

The overall objective of the optimization is to establish the position on the plate that experiences the greatest accumulated strain over the entire frequency range. However, as previously discussed, the strain generated in the plate is a function of the deflection of the plate in both *x* and *y* directions and therefore both directions of strain must be considered simultaneously. This will ultimately result in not only an optimal position but an optimal orientation of the harvester at that position. This is important to ensure the maximum power from a vibrating plate is to be achieved because, as previously highlighted, the power generated by a piezoelectric transducer is related to the direction of strain with respect to the piezoelectric's poling direction. The orientation of the maximum strain at any position can be determined from its two components: the maximum strain in the x direction and the maximum strain in the y direction, using the formula

$$\varepsilon_{max} = \pm\varepsilon_x cos\theta \pm \varepsilon_y sin\theta \tag{9}$$

where ε_{max} represents either the maximum bending or membrane strain and ε_x and ε_y are the corresponding bending or membrane strains in the *x* and *y* directions respectively.

Equation (9) gives the objective function for the placement of one harvester on a panel based on the strain at its center. In this work we consider a set of four harvesters leading to the objective function given by Equation (10)

$$\varepsilon_{max} = \sum_{i=1}^{4} \pm \varepsilon_{x} cos\theta \pm \varepsilon_{y} sin\theta \quad (10)$$

Location optimization

The optimization process was performed using SolveXL, a genetic algorithm add-in for Excel. The details of the GA used are given in Table 4.

Table 4. Genetic algorithm

Algorithm:	NSGA2
Population size:	100
Number of Generations:	1000
Cross over:	Simple Multi-point
Selector:	Crowded Tournament
Mutator:	Simple by gene
Real bound integers	
Limits	
Panel dimensions:	254 x 387
X location of harvester:	27.5<x<359.5 (panel length – length of harvester)
Y location of harvester	27.5<y<226.5 (panel width – length of harvester)
Angle of harvester:	0<θ<2π

Penalty case: if any two harvester pairs are within a radius of 55mm (greatest dimension of harvester) of each other a penalty was added to the solution which meant it was no longer valid. This prevented harvesters being placed on top of each other etc.

The GA program was used multiple times with the cross over rate and mutation rate altered from 0.8 to 0.95 and from 0.05 to 0.25 respectively. The best solution from each run was recorded, and then all the solutions were analyzed which allowed clustering into groups of solutions based on the harvester position from the center of the panel. Once the groups of solutions had been determined, any symmetry within the harvester co-ordinates was removed so that all harvesters were located within the same four positions. Finally an average of each solutions was taken to derive the actual harvester location and orientation.

Optimized harvester positions

Figure 4 shows an example set of solutions from the GA program.

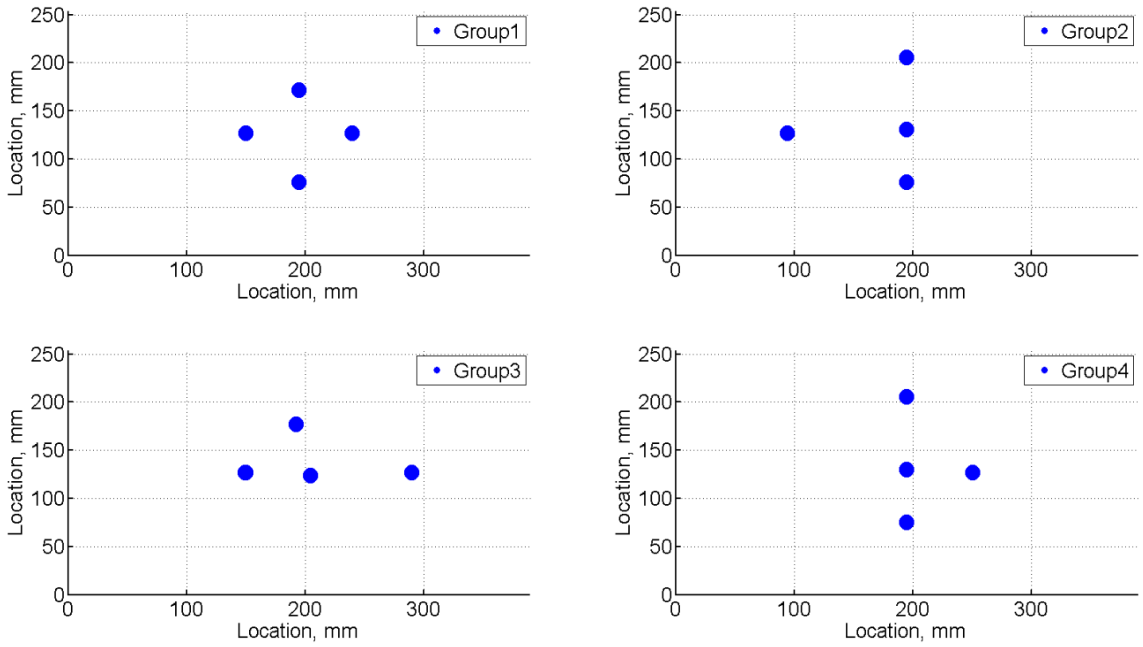

Figure 4. Energy harvester locations groups resulting from the optimisation programme

Figure 5 shows the variation in the predicted summation of the numerical strain for each location group. It can be seen from this that there is very little difference in total strain levels for each group.

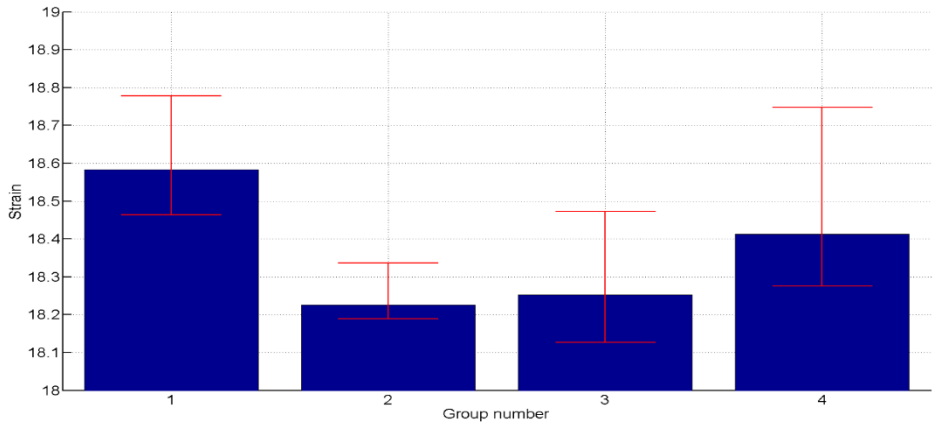

Figure 5. Predicted numerical strain for each location group

Table 5 and Figure 6 show the initial, non-optimized harvester locations which were based solely on an inspection of the identified mode shapes and an estimate of the best locations for these and the optimized locations for group 4 which were chosen to be validated experimentally. It can be seen that the optimized solutions increase the predicted strain levels by a factor of two.

Table 5. Comparison of non-optimized and optimized harvester locations

	Non-optimized Positions		Optimized Positions	
	Harvester co-ordinates (mm)	Angles, °	Harvester co-ordinates (mm)	Angles, °
EH1	(193.5,127)	0	(196.8,128.5)	238.96
EH2	(193.5,190.5)	0	(194.3,75.4)	46.01
EH3	(292.25,127)	0	(130.0,127)	60.16
EH4	(292.25,190.5)	0	(194.5,205.1)	240
Predicted strain	9.31		18.62	

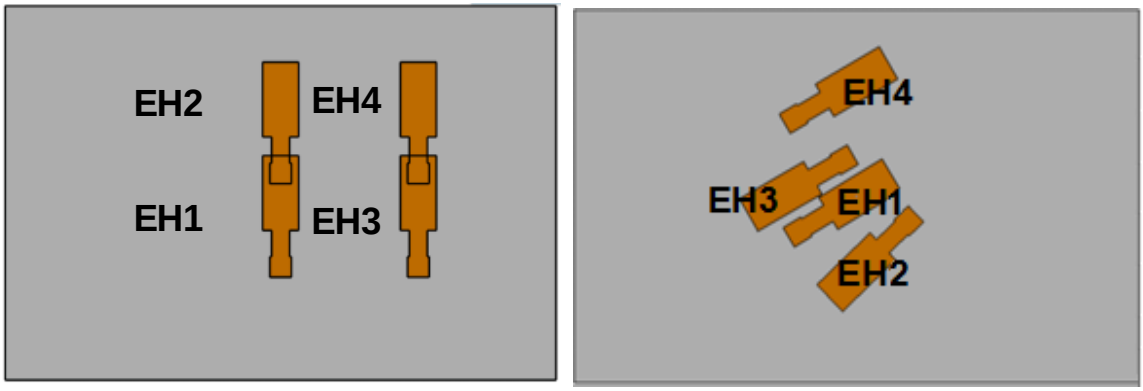

Figure 6. a) Original and b) optimized energy harvester locations

Experimental validation

Experimental set-up

A series of tests were performed to validate the optimization process. Two panels were prepared, one with harvesters in the non-optimized positions and one in the positions calculated by the GA. For each, four Mide QP10ns (Figure 7) chosen after consideration of the range of harvesters shown, were bonded to a 437mm x 304mm panel (387mm x 254mm unsupported plus 25mm along each edge to allow for clamping) using Vishay group M-Bond AE-10 strain gauge glue following the guidelines in the manufacturer's data sheet. Characteristics of this actuator and the others considered are given in Table 6.

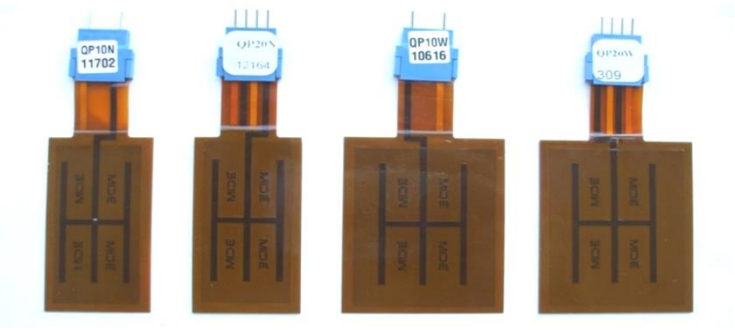

Figure 7. Mide QP10n, QP10w, QP20n and QP20w piezoelectric transducers

Table 6. Mide QP10n, QP10w, QP20n and QP20w characteristics

Product	QP10n	QP10w	QP20n	QP20w
Piezo Layers	1 x 10-mil [US]	1 x 10-mil [US]	2 x 10-mil [US]	2 x 10-mil [US]
Device Size [in]	2.00 x 1.00 x 0.015	2.00 x 1.50 x 0.015	2.00 x 1.00 x 0.03	2.00 x 1.50 x 0.03
Active Size [inches]	1.81 x 0.81 x 0.01	1.81 x 1.31 x 0.01	2 x (1.81 x 0.81 x 0.01)	2 x (1.81 x 1.31 x 0.01)
Weight [oz]	0.1	0.1	0.17	0.28
Capacitance [μF]	0.06	0.06	0.12	0.20
Voltage Range [V]	± 200	± 200	± 200	± 200
Full-scale Strain [με]	± 262	± 278	± 264	± 280

The panel was tested using the rig shown in Figure 8. Two rectangular frames manufactured from 25x25mm mild steel were bolted together through the panel thereby clamping its edges in place and restricting all translations and rotations. These frames were mounted on a box made from 5mm thick mild steel plate to allow the connection of an electromagnetic (EM) shaker to the center of the panel from underneath. The frame

had a mass of approximately 22kg and was designed in order to prevent the loss of vibration energy due to the displacement of the rig. The shaker used to vibrate the panel was a V201 EM shaker from LDS. The oscillating section of the shaker was connected to the panel using an extendable connecting arm. The fixed section, which was made of brass, was bonded to the center of the underside of the panel using Loctite 330 adhesive and then screwed into the shaker.

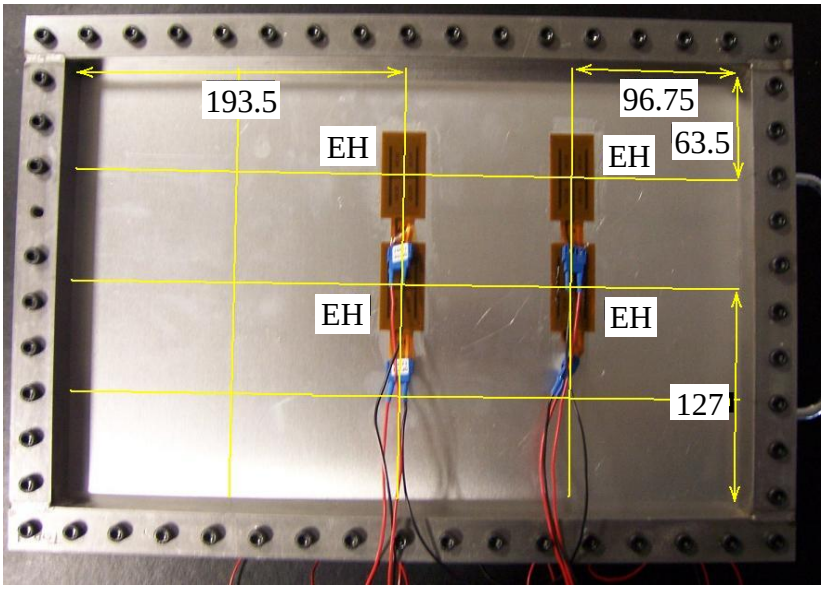

Figure 8. Harvester positions (all dimensions in mm)

The frequency and amplitude of the signal for the vibration were specified using a dedicated user interface developed within the software LabVIEW from National Instruments (NI) and produced by an NI USB-6211 bus. This signal was amplified using a PA25E amplifier (also from LDS) to transform the signal to that required for powering the EM shaker (Figure 9).

In order to control the amplitude of vibration, a height measuring rod was set up at the required height above the EM shaker, the top of which sat at the mid-point of vibration when stationary. The amplitude gain on the amplifier was set to a known constant level, and the amplitude setting was varied using the LabVIEW controls until the setting which brought the shaker top up to the height measuring rod was found.

The energy harvesters were connected back through the NI USB-6211 bus used to produce the vibration signal, to a desktop computer. LabVIEW software was again used for data acquisition, to record the signals produced by the energy harvesters, and to export the logged information into Microsoft Excel spreadsheets for analysis.

Figure 9. Experimental set-up

The panel was vibrated at frequencies up to 400Hz to cover the 0 – 350Hz range anticipated in flight. Each piezoelectric patch was connected to the resistance junction box in parallel and an oscilloscope was used to measure the voltage for the given resistance value. For a given frequency the load resistance was altered from open circuit to 20kΩ. This process was repeated in a round robin configuration connecting a single patch to the resistance box for a given frequency and then repeated for all frequency measurements. The power was calculated based on the measured voltage for each resistor.

Validation

The experimental vibration amplitudes achieved at each harvester position across the range of frequencies tested were first determined using a Polytec PSV-500-3D scanning laser vibrometer and are shown in Figure 10. These are clearly significantly smaller than those expected in a typical aircraft panel (max 10 μm achieved against a desired amplitude of +/- 0.2mm) due to the power rating of the actuator. This will clearly affect the level of energy harvested however it will still provide the means to compare the energy harvested by the non-optimized and optimized set-ups.

The vibrometer data was also used to derive full field diplacment plots at the resonant frequencies in order to compare the experimental mode shapes with those used in the model. The results of the first three mode shapes are shown in Figure 11. Whilst the natural frequencies measured are lower than those predicted due to simplifications made in the model (e.g. ignoring the effects of damping, idealised boundary conditions) the experimental results confirm the mode shapes expected are replicated using the actuator bonded to the centre of the panel.

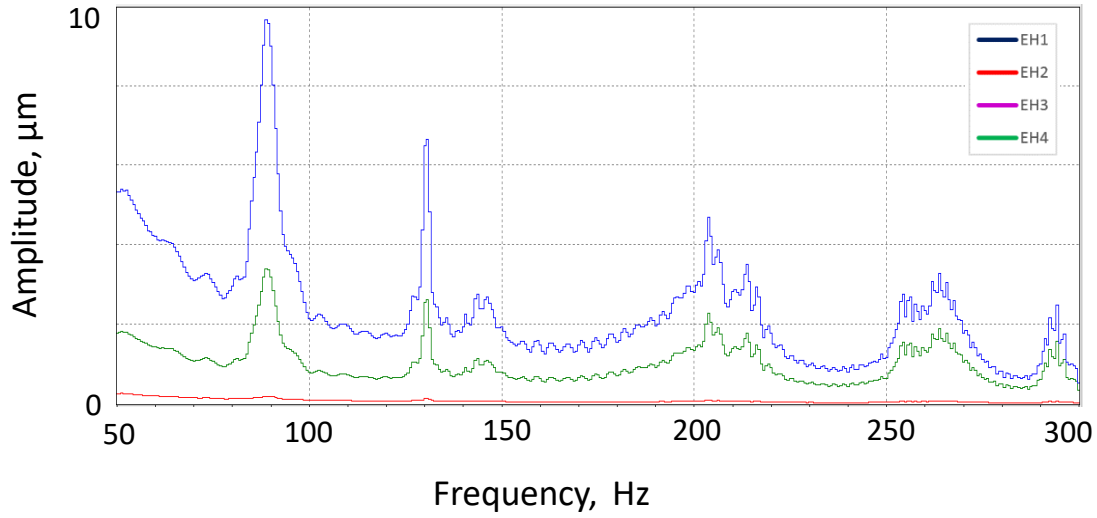

Figure 10. Vibration amplitudes

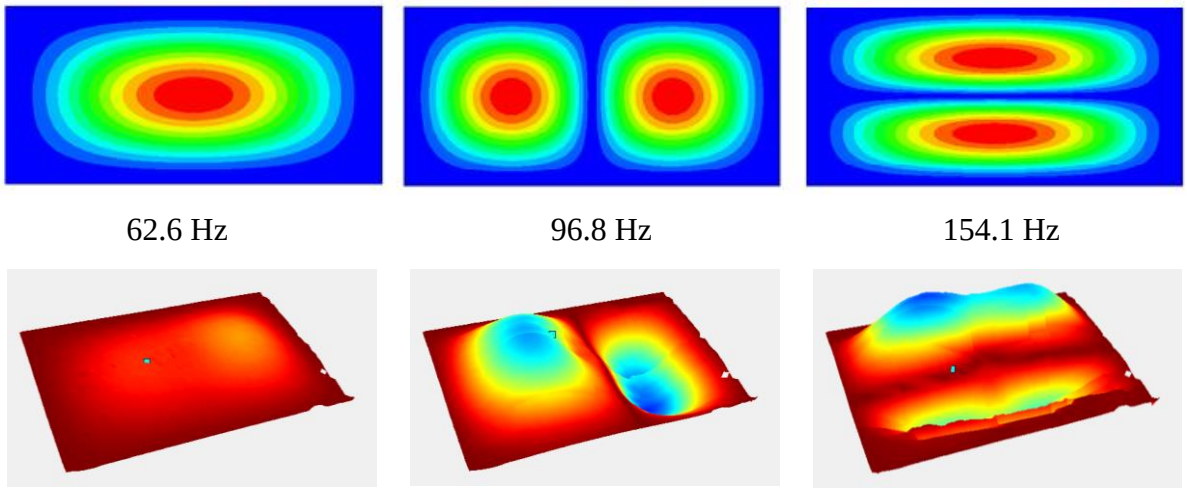

Figure 11. Mode shapes corresponding to the first three natural frequencies of the panel a) model and b) experimental

Results

Figure 12 shows the resulting RMS power for each vibrational frequency with maximum power levels of 9mW being harvested for the optimised harvester configuration. Unfortunately in this configuration EH2 became damaged during bonding and therefore

had to be omitted from the test, this was confirmed by a dramatic reduction in capacitance of this particular harvester.

Figure13 shows the resulting load resistances for matched power transfer which demonstrate a reduction in resistance for an increase in frequency. This highlights the importance of accounting for this in the power management circuitry.

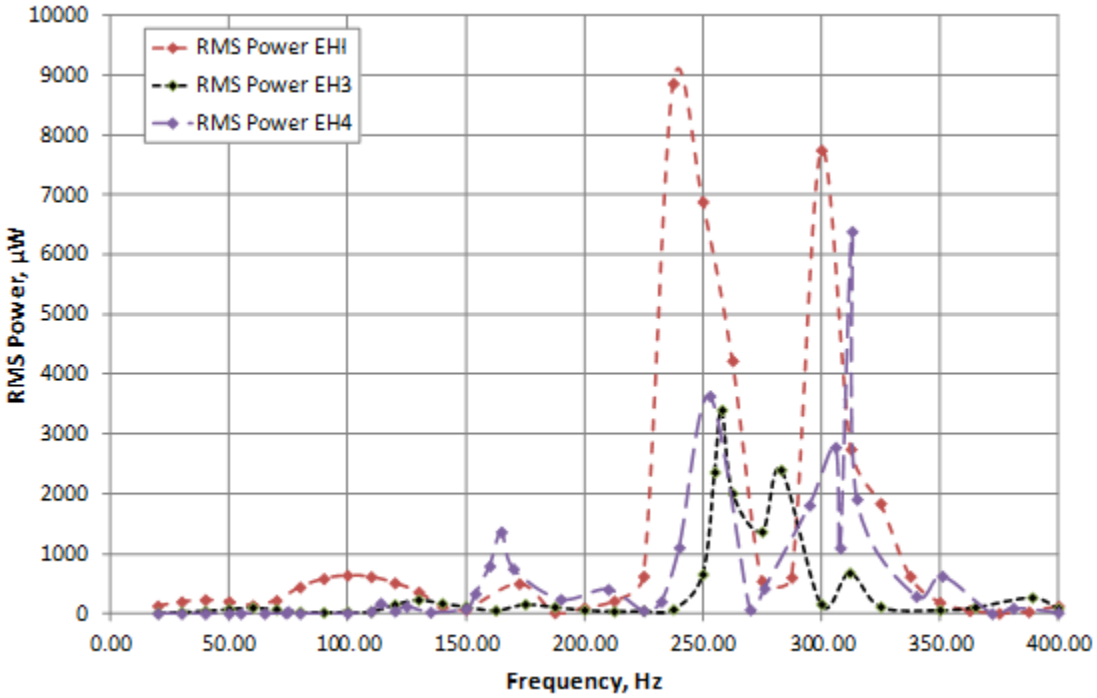

Figure12. Harvested power for each energy harvesting device

Discussion

The theoretical values of mean harvested power for each of the energy harvesters in their original positions (prior to optimization) averaged across the frequency bandwidth and the corresponding values for the harvesters in their optimized positions is presented in Figure 14 and Table 7. These show considerable increases in mean power for each harvester location when compared with the non-optimized solution with a predicted doubling of the energy harvested.

The corresponding experimental data for frequencies between 0 and 350Hz frequency range can be seen in Figure 15 and Table 8. Unfortunately there is no data for EH2 for the optimized position due to damage suffered during the bonding process. Despite this, the optimized layout gives an increase in power from 1466µW to 2071µW for the group and the average power per harvester is increased from 388µW for the non-optimized

configuration to 690µW for the optimized position therefore demonstrating a significant improvement. Since the theoretical results predict that EH2 will generate significantly more power than EH3 and EH4 it is likely that the complete set would generate a higher average output than this.

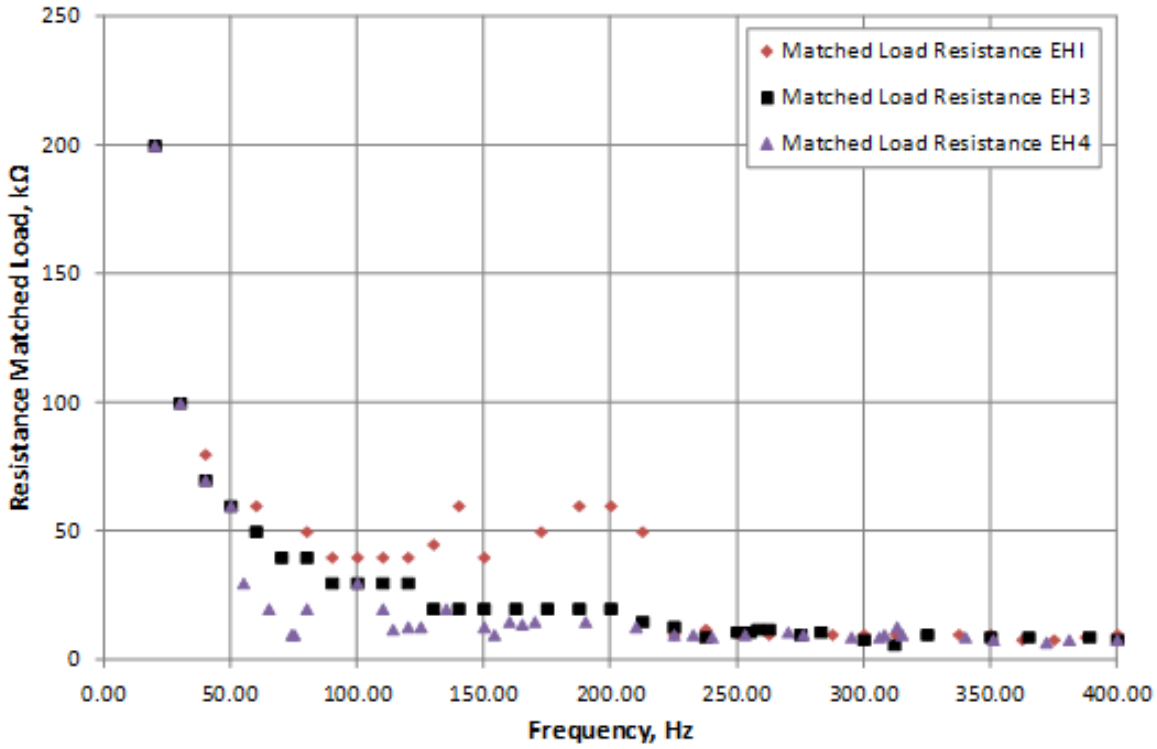

Figure13. Resulting matched load for each frequency for maximum power transfer

Comparing with the power requirements presented previously - 16 mW operating and 0.12mW sleep it can be seen that sufficient power could be generated to support the system in sleep mode, with further optimisation of the system required to generate the full 16mW. It should be noted however, that it is likely that the sensor node would be powered based on a combination of different harvesting techniques, and that the role of the vibration harvesting would be to provide continuous, lower levels of power to supplement discontinuous power coming from for example thermal gradients which change over the duration of the flight.

Whilst both the theoretical and measured power outputs are based on a particular structure with assumptions made regarding the amplitude and frequency of vibration and the number of harvesters used, the methodology proposed would be applicable in a number of other scenarios. For example composites, which could potentially have a significant effect on vibration mode shapes and natural frequencies and would clearly have an impact on the positioning of the piezoelectric patches and the power harvested could be incorporated into the model by rewriting the strain expressions to take into

account anisotropy. This could potentially be advantageous if it resulted in bistable behaviour which enhanced harvesting over a broad band of frequencies. Differing levels of vibration energy would result in different deflection amplitudes which could again be incorporated into the calculations. Different numbers of harvesters could be used considering the need to balance the cost and complexity of the system with the probability of detection and the power requirements.

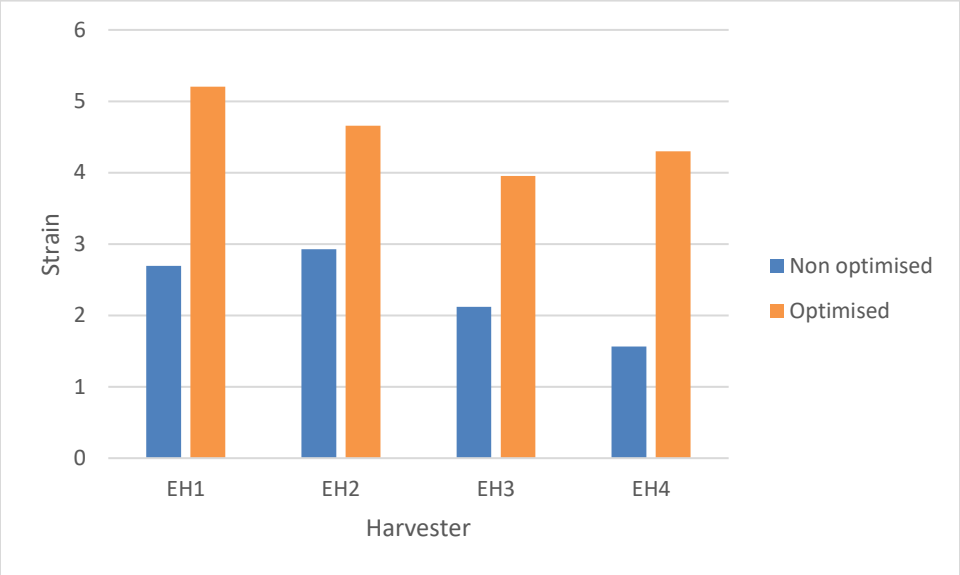

Figure 14. Theoretical average strain at harvester locations before and after optimization

Table 7. Theoretical strain for optimised and non optimised layout

	Non-optimised layout	Optimised layout
EH1	2.69	5.21
EH2	2.93	4.66
EH3	2.12	3.95
EH4	1.57	4.30
Total	9.31	18.12

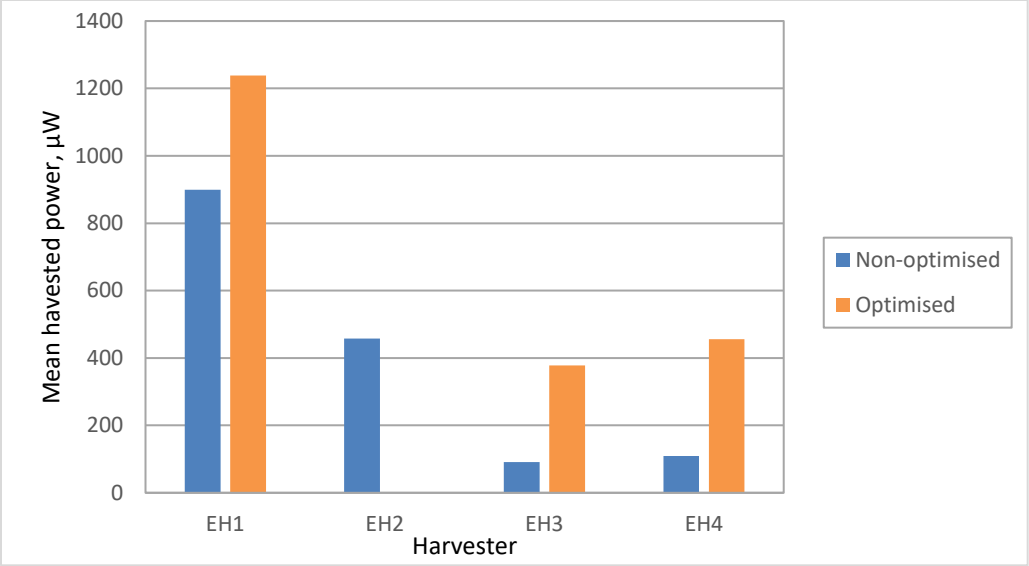

Figure 15. Mean harvested power across the frequency bandwidth at harvester locations before and after optimization

Table 8. Mean harvested power for optimised and non-optimised layout

	Non-optimized (µW)	Optimized (µW)
EH1	898.79	1238.06
EH2	457.71	-
EH3	90.79	377.46
EH4	109.24	455.37
Total	1466	2071

Conclusion

The positions of a series of piezoelectric harvesters mounted directly on a panel representative of an aircraft wing panel have been optimized to harvest vibration energy over the range of frequencies it is expected to experience during flight in order to power a Structural Health Monitoring System node. The optimization was based on maximizing the strain at the harvester locations by considering the mode shapes of all the natural frequencies which fall within the expected frequency range and using a genetic algorithm based technique. Theoretical results showed an increase in strain over four harvesters of 100% from their original position. Experimental validation work demonstrated a 50%

increase in power harvested despite one of the harvesters (which was predicted to be one of the most effective) being damaged and therefore inoperable.

Thus this work has shown the potential to harvest vibration energy directly from an aircraft structure, avoiding the additional mass and complexity which would be introduced by a retrofitted cantilever harvester such as those most frequently used for vibration harvesting, which can be maximized by optimal placing of these harvesters. By considering the full range of modes in which the panel vibrates a more broadband harvesting profile can be achieved.

Going forward it will be essential to optimize the location of both the sensor nodes and the co-located harvesters in a multi-objective optimization based on the sensor nodes (minimizing the number of nodes whilst maximizing probability of detection (PoD)) and the harvester location (maximizing energy harvested). This will need to take into account that whilst the sensors and harvesters need to be co-located to avoid additional wiring and losses, the optimum location for the sensor may not be the optimum location for the harvester.

References

Anton SR, Erturk A and Inman DJ (2012) Multifunctional unmanned aerial vehicle wing spar for low-power generation and storage. *Journal of Aircraft* 49(1): 292-301.

Anton SR and Inman DJ (2011) Performance modelling of unmanned aerial vehicles with on-board energy harvesting. *Proceedings of the SPIE* 7977(79771H).

Bachmann F, Bergamini AE and Paolo E (2012) Optimum piezoelectric patch positioning: A strain energy based finite element approach. *Journal of Intelligent Material Systems and Structures* 23(14): 1575-1591.

Chidambaram N, Mazzalai A. and Mural P (2012) Measurement of effective piezoelectric coefficients of PZT thin films for energy harvesting application with interdigitated electrodes. *IEEE Transactions on Ultrasonics, Ferroelectrics and Frequency Control* 59(8): 1624-1631.

Ertuk A (2009). Piezoelectric energy harvesting from multifunctional wing spars for UAVs - Part 1: Coupled modelling and preliminary analysis. *Proceedings of the SPIE* 7288(72880C).

ESDU 1995. Natural frequencies of rectangular flat plates with various edge conditions.

ESDU. 1996. Design against fatigue: vibration of structures under acoustic or aerodynamic excitation.

ESDU. 1968. Atmospheric data for performance calculation.

Fang HB, Liu JQ, Xu ZY, et al. (2006). Fabrication and performance of MEMS-based piezoelectric power generator for vibration energy harvesting. *Microelectronics Journal* 37(11): 1280 - 1284.

Ferrari M, Ferrari V, Guizzetti M (2010) Improved energy harvesting from wideband vibrations by nonlinear piezoelectric converters. *Sensors and Actuators A: Physical* 162(2): 425-431.

Grigg, S (2018) Development of a wireless structural health monitoring system for aerospace application. *PhD Thesis, Cardiff University*.

Jegely DC (1998) Behavior of compression-loaded composite panels with stringer terminations and impact damage. AIAA/ASME/ASCE/AHS 39th Structures, Structural Dynamics, and Materials Conference, Long Beach, California.

Karami MA, Farmer, JR and Inman DJ (2013) Parametrically Excited Nonlinear Piezoelectric Compact Wind Turbine. *Renewable Energy* 50: 977-987.

Kim JK, Zhou D, Ha DS, et al. (2009) A practical system approach for fully autonomous multi-dimensional structural health monitoring. *Proceedings of the SPIE: Sensors and Smart Structures Technologies for Civil, Mechanical, and Aerospace Systems* 7292(72921L).

Liao Y and Sodano HA (2012) Optimal placement of piezoelectric material on a cantilever beam for maximum piezoelectric damping and power harvesting efficiency. *Smart Materials and Structures* 21(10): 1-9.

Liu H, Quan C, Tay CJ, et al. (2011). A MEMS-based piezoelectric cantilever patterned with PZT thin film array for harvesting energy from low frequency vibrations. *Physics Procedia: 2011 International Conference on Optics in Precision Engineering and Nanotechnology* 19:129 - 133.

Ly R, Rguiti M, D'Astorg S, et al. (2011) Modelling and characterization of piezoelectric cantilever bending sensor for energy harvesting. *Sensors and Actuators A: Physical* 168(1): 95-100.

Mascarenas D L, Todd MD, Park G, et al. (2007) Development of an impedance-based wireless sensor node for structural health monitoring. *Smart Materials and Structures* 16(1): 2137 - 2145.

Ng TH and Liao WH (2005) Sensitivity analysis and energy harvesting for a self-powered piezoelectric sensor. *Journal of Intelligent Material Systems and Structures* 16(10): 785-797.

Pasquale GD, Soma A and Fraccarollo F (2011) Piezoelectric energy harvesting for autonomous sensors network on safety-improved railway vehicles. *Proceedings of the Institution of Mechanical Engineers, Part C: Journal of Mechanical Engineering Science* 226(4): 1107 - 1117.

Sodano HA, Inman DJ and Park G (2005) Comparison of piezoelectric energy harvesting devices for recharging batteries. *Journal of Intelligent Material Systems and Structures* 16(10): 799 - 807.

Sodano HA, Lloyd J and Inman DJ (2006) An experimental comparison between several active composite actuators for power generation. *Smart Materials and Structures* 15(5): 1211 - 1216.

Thangaraj, Karthik 2017. Development of efficient energy storage and power management for autonomous aircraft structural health monitoring systems. *PhD Thesis, Cardiff University.*

Timoshenko SP and Woinowsky-Krieger S (1959) Theory of plates and shells. Singapore: McGraw-Hill Inc.

Wu J, Yuan S, Zhao X, et al. (2007) A wireless sensor network node designed for exploring a structural health monitoring application. Smart Materials and Structures 16(5): 1898 - 1906.

Zhou D, Kim JK, Bile LK, et al. (2009) Ultra-low-power autonomous wireless structural health monitoring node. Structural Health Monitoring 2009: Proceedings of the Seventh International Workshop on Structural Health Monitoring 1: 797 - 804.

Zhu D, Beeby SB, Tudor MJ, et al. (2011) A credit card sized self-powered smart sensor Node. *Sensors and Actuators A: Physical* 169(2).

Zhu M and Edkins S (2011) Analytical modelling results of piezoelectric energy harvesting, Devices for Self-Power Sensors/Sensor Networks in Structural Health Monitoring. *Procedia Engineering* 25: 195-198.